The Astronomical Journal, 142:179 (15pp), 2011 December doi:10.1088/0004-6256/142/6/179

VARIABLES IN GLOBULAR CLUSTER NGC 5024

M. Safonova and C. S. Stalin
Indian Institute of Astrophysics, Koramangala, Bangalore 560 034, India; rita@iiap.res.in, stalin@iiap.res.in
Received 2011 May 21; accepted 2011 August 16; published 2011 October 20

ABSTRACT

We present the results of a commissioning campaign to observe Galactic globular clusters for the search of microlensing events. The central $10' \times 10'$ region of the globular cluster NGC 5024 was monitored using the 2 m Himalayan Chandra Telescope in *R*-band for a period of about 8 hr on 2010 March 24. Light curves were obtained for nearly 10,000 stars using a modified Differential Image Analysis technique. We identified all known variables within our field of view and revised the periods and status of some previously reported short-period variables. We report about 70 new variable sources and present their equatorial coordinates, periods, light curves, and possible types. Out of these, 15 are SX Phe stars, 10 are W UMa-type stars, and 14 are probable RR Lyrae stars. Nine of the newly discovered SX Phe stars and one eclipsing binary belong to the blue straggler star population.

Key words: blue stragglers – globular clusters: general – globular clusters: individual (M53) – stars: variables: general

1. INTRODUCTION

With the recent discovery that most galaxies host massive black holes in their centers, the question was raised regarding the detection of such central black holes in low-mass, non-active stellar systems, of which globular clusters (GCs) are potential candidates. The well-established correlations between the properties of supermassive black holes and their host galaxies do suggest that, by extrapolation, GCs follow the same relations (Safonova & Shastri 2010). Most of the attempts to search for the central intermediate-mass black holes (IMBHs) in GCs, however, are not direct and present enormous observational difficulties due to the crowding of stars in the GC cores. Recently, Safonova & Stalin (2010) proposed a method for detecting the central IMBH in GCs by microlensing (ML) of the cluster stars. In 2010, we have initiated the observational program to search for ML signatures using the 2.0 m Himalayan Chandra Telescope (HCT) at the Indian Astronomical Observatory (IAO), Hanle, and the 2.3 m Vainu Bappu Telescope at the Vainu Bappu Observatory, Kavalur, both operated by the Indian Institute of Astrophysics (IIA), Bangalore. The program consists of obtaining one set of observations each in the *V* and *I* bands of a selected set of clusters every 15–20 days for a period of 5–7 years (Safonova & Stalin 2010). The GC NGC 5024 (M53) was observed as part of the commissioning observations for this program.

It is well known by now that any ML search yields a data set suitable for detecting variable stars that are unrelated to ML events (see, for example, Cook et al. 1997). Moreover, it was also discovered that the regular ML observations are more efficient at finding faint variables, being insensitive to bright ones because of saturation. In this paper, we report the results of the commissioning observations of our IMBH campaign. Out of the whole set of GCs from the main campaign, GC M53 was chosen because it was accessible at the time of observation and because of its high variable content. The data set presented in this paper is not identical to our main ML time-series data set. We used these observations to tune our data-reduction pipeline, to build the analytical tools for investigation of our full time-series database, and to test our ability to obtain high-quality photometry in order to retrieve variable signals with the timescales and depth of typical GC stellar variability.

M53 ($\alpha_{2000} = 13^{\rm h}12^{\rm m}55\overset{\rm s}{.}3$, $\delta_{2000} = +18^{\circ}10'9''$) is a moderately compact, metal-poor ([Fe/H] $= -2.04$; Zinn 1985), outer halo GC that is rich in RR Lyrae variables. Though M53 has been photometrically searched for variability several times since 1998 (Rey et al. 1998; Kopacki 2000; Jeon et al. 2003; Dekany & Kovacs 2009), only variables of a pulsating type have been found. In the latest 2010 updated version of the catalog of variables in M53 (Clement et al. 2001) there are 62 reported RR Lyrae (RRl) stars, 8 suspected long-period semi-regular (SR) stars, and 15 reported SX Phe stars. Out of almost 200 blue straggler stars (BSSs) discovered so far in M53, 14% is estimated to be in binary systems (Beccari et al. 2008); however, no eclipsing binaries were previously found in this cluster.

Despite the high variable content of M53 and a favorable position in the galaxy where both field contamination and interstellar reddening are very low, $E(B - V) = 0.02$ (Schlegel et al. 1998), the only extensive time-series photometry study has been done recently by Dekany & Kovacs (2009, hereafter referred to as DK). Previous studies used point-spread function (PSF) fitting directly to the images. Though this method performs well in crowded fields compared to aperture photometry, Differential Image Analysis (DIA) is better suited for time-series observations searching for variables in very crowded fields like GCs, as the changes in the seeing during the course of the observations are well accounted for. In this present work, we apply a new pipeline based on an improved version of the differential imaging analysis, developed by Bramich (2008), to a set of *R*-band images in order to search for variables down to $R = 21$ mag. We have recovered all previously known variable stars in our field of view (FOV) and revisited all known short-period SX-Phe-type stars in an attempt to refine their periods and coordinates. We report new candidate variables, determine the periods of new short-period variable (SPV) stars, and report candidate eclipsing binaries and flux variability amongst some of Stetson's photometrically standard stars. Some of the new variables were matched to the BSS stars discovered earlier by Beccari et al. (2008). The emphasis of this work is on reporting the new SPV sources. The final characterization of the newly discovered variables, especially the detailed photometry of matched BSSs based on their position on the color–magnitude diagram to estimate mass and

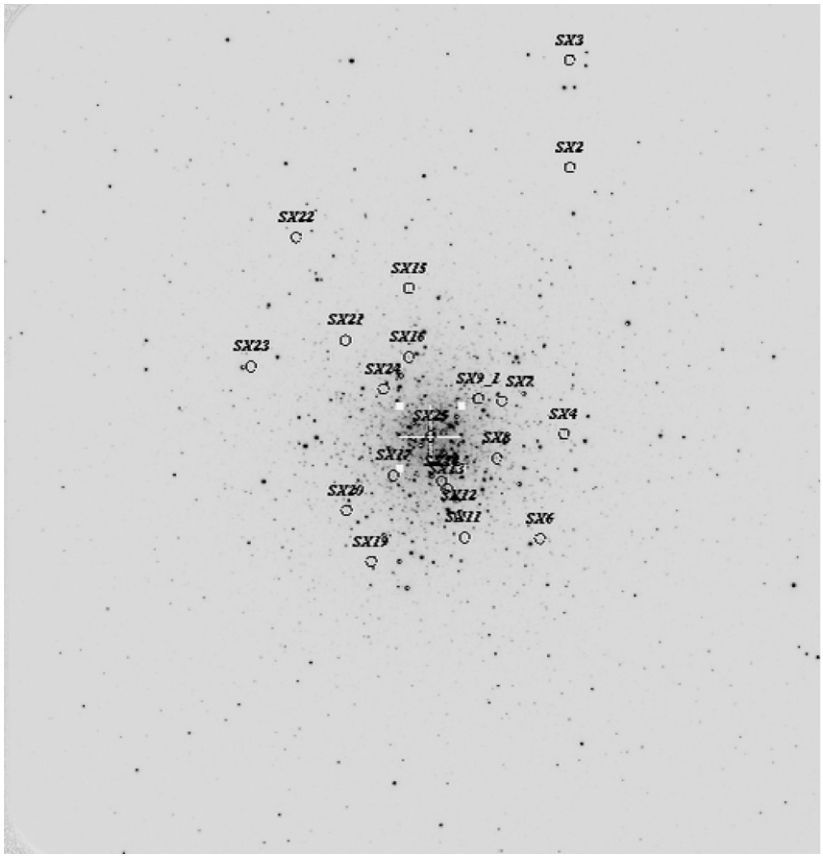

Figure 1. 10 × 10 arcmin^2 grayscale map of an *R* reference image of the globular cluster M53. Sixteen confirmed SX Phe stars are labeled by their respective designations given in Table 6. The image was scaled only to mark the positions of the stars. The cross marks the center of the cluster. The cluster size is ∼13′; thus we can be confident that most detected variables belong to the cluster. North is up, east to the left.

temperature from isochrone fitting, will be presented in a future paper. This paper is structured as follows. Observations and data reduction are described in Section 2. In Section 3, we discuss previously known variables in M53; in Section 4 we describe the search for new variables, explain the methods we used to identify new variable stars (RR Lyrae, SX Phe, eclipsing binaries), list the properties of all newly detected variables, and display their light curves; and in Section 5 we give the summary of our results.

2. OBSERVATIONS AND DATA REDUCTION

2.1. Observations

Photometric data were obtained on 2010 March 24, using the Himalayan Faint Object Spectrograph and Camera (HFOSC) mounted on the 2.0 m HCT of the IAO, located 4500 m above sea level. A total of 101 image frames, each of 100 s exposure, were collected in *R*-band during continuous 8 hr of observations. HFOSC is equipped with a SITe 2048 × 4096 thinned back-illuminated CCD. We have used the central 2048 × 2048 pixel region for imaging, with a pixel scale of 0.″296 pixel^{-1} and an FOV of ∼10′ × 10′. The readout noise, gain, and readout time of the CCD are 4.8 $\bar{e}$, 1.22 $\bar{e}$/ADU, and 90 s, respectively. Observations were done under photometric sky conditions with typical seeing of about 1.5 arcsec.

A gray-scale map of an *R* CCD image (reference frame, RF) is shown in Figure 1. It shows an area of about 10′ × 10′ observed field. Sixteen confirmed SX Phe stars are represented by circles labeled with their respective designations given in Table 6. A first indication of whether a star detected in the field of a GC belongs to this cluster is its location with respect to the center of the cluster. The tidal radius of M53 is 21.75 arcmin (Harris 1996), and hence all newly found variables are well within the tidal radius.

2.2. Data Reduction

To extract high-precision photometry from the M53 image frames, we employed the DIA technique implemented through a pre-release version of the pipeline DanDIA[1] (Bramich 2008). The idea of DIA is to obtain information about the brightness behavior of a source by analyzing the difference between the image in each of the frames from the time series and the image in an RF. This technique allows the extraction of high signal-to-noise ratio (S/N) signals even in the highly crowded central regions of GCs (Alard & Lupton 1998; Alard 2000; Bramich et al. 2005; Bramich 2008). The DanDIA pipeline is well described in a series of papers by Arellano Ferro et al. (2008).

Briefly, the raw image data are passed through a series of modules, starting with bias subtraction, flat-field corrections, and cosmic ray removal. The gain and readout noise at the time of observations were calculated automatically at the first stage. An RF was chosen out of the best-seeing pre-processed images in which the FWHM of the PSF was measured to be ∼3.77 pixels. A series of difference images was created by subtracting the RF from each registered image. Photometry on the difference images via optimal PSF scaling (Bramich et al. 2005)

[1] DanDIA is build from the DanIDL library of IDL routines (http://www.danidl.co.uk).

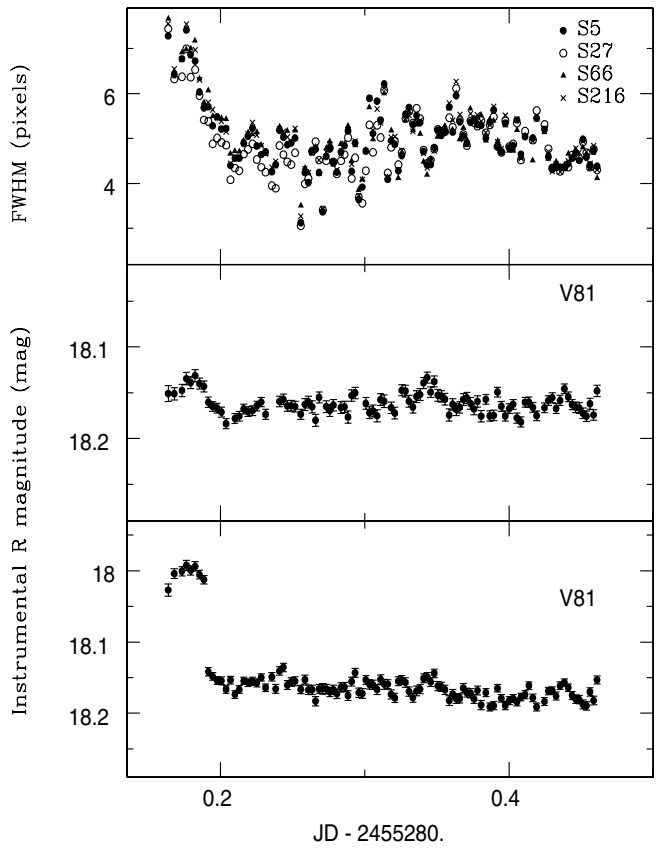

Figure 2. Top panel: changes of the FWHM of four of Stetson's (2000) standard stars, S5, S27, S66, and S216, with *R* magnitudes of 13.9, 14.5, 17.3, and 16.3 mag, respectively. Middle and bottom panels: the light curves of a star, V81, obtained on running the DanDIA subtraction module with a 6 × 6 and a 3 × 3 subdivision grid, respectively.

yielded the light curves of differential fluxes for approximately 10,000 stars.

2.3. Problems with Data Reduction

During the data-reduction stage, we have discovered two features of the differential image construction with DanDIA that had effects on the photometry of some stars. First, as was described in Bramich et al. (2011), due to the saturation effects on the RF, DanDIA rejects the area in the difference image around the saturated star. As a result, in the neighborhood of saturated stars it may be impossible to extract any photometric measurements. We have reduced the exposure time as much as possible without degrading the S/N to minimize the number of saturated stars. However, our images still contain several saturated stars, which could have affected the photometry of nearby candidates. Consequently, we discarded any candidate variables that were closer than 10 pixels to such stars.

Second, at the stage of variable selection, we found that a large number of stars had nearly identical light curve variations correlated in time. In many cases this false variability was also correlated with the intra-night changes in PSF. In the top panel of Figure 2, we display the changes of the FWHM (in pixels) of the four photometric standard stars (Stetson 2000) located at different positions on the CCD.

We suspect that the origin of this effect may be due to the combination of the intra-night changes of the stellar PSF and the way DIA works. It is possible that this variability is induced at the subtraction stage. A distinctive feature of any DIA software is a subdivision of each registered image into a grid of subfields, each of which can take on different values for the parameters that are used to convolve the reference image with the kernel for image subtraction. Thus, when DanDIA convolves the RF with other frames, a set of kernels are derived matching each image subregion to the corresponding subregion in the RF (Bramich 2008); but for each subregion of the grid, DanDIA uses different parameters. It is possible that at the edges of these subregions DanDIA finds it difficult to fit the convolution parameters. For stars situated in those areas, the intra-night PSF changes could result in inadequate convolution that may show up as photometric variability. This kind of problem was also reported by Pepper et al. (2008) due to the considerable intra-night drift of their telescope pointing. In an attempt to remedy this, after the initial run of the subtraction stage with a grid of 6 × 6 subdivisions, we had a re-run with the coarser grid of 3 × 3 subregions and found induced changes in the light curves of some stars that were previously non-variable. For example, the star V81 reported by DK was found by us to be non-variable on the initial run of the pipeline (Figure 2, middle panel and Section 3.2). On the re-run, it started exhibiting a spurious variability of the type mentioned above, which is clearly seen in Figure 2 (bottom panel). It is possible that during the re-run, this star turned out to be on the edge of the subregion while previously it was away from it. It is difficult to determine in advance any false variability due to this effect, thus we have rejected such light curves through a visual examination of variable candidates.

2.4. Astrometric and Photometric Calibration

The astrometric transformation between the pixels and celestial coordinates for the RF was done using 46 photometric standard stars in the field of M53, taken from P. Stetson's online catalog (Stetson 2000) at the Canadian Astronomical Data Center (CADC),[2] which were uniformly distributed around the cluster center and located sufficiently outside the cluster core. Since our observations were performed at the current epoch of J2010.235873, we first precessed the coordinates of these standards from the J2000.0 epoch to the epoch of our observation (using the IRAF utility *precess*), calculated the transformation solution from pixel to equatorial coordinates (α, δ), and then precessed the solution back to epoch J2000.0. The standard deviations in the residuals of the coordinate transformation were $0\farcs052$ and $0\farcs053$ in right ascension and declination, respectively. We have found that in 10 years (from J2000.0 to J2010.225873), the cluster has moved by $470\farcs2$ ($450\farcs57$ in α and $-194\farcs59$ in δ). This is more or less consistent with the precession value of 1° per 72 years ($50''$ yr^{-1}). The cluster's proper motion was estimated earlier to be very small, $\sim 0.5 \pm 1$ mas yr^{-1} (Dinescu et al. 1999).

Out of these 46 photometric standard stars, 24 were used to obtain the absolute photometric calibration. The standard *R* magnitudes for these stars were obtained from the online USNO-A2.0 Catalogue Server (http://archive.eso.org/skycat/servers/usnoa) and the mean between the standard magnitude $R_{\rm std}$ and the instrumental magnitude $r_{\rm inst}$ was calculated, $\Delta m = -0.79 \pm 0.25$. This mean was used to obtain the standard *R* magnitudes of all new variables found in this study. The standard deviation of 0.25 mag in our photometric zero point is

[2] The catalog is available at http://www3.cadc-ccda.hia-iha.nrc-cnrc.gc.ca/community/STETSON/standards/.

mainly due to the 0.3 mag photometric accuracy in the USNO magnitudes (Monet et al. 2003).

3. VARIABLE STARS IN M53

According to the updated 2010 online version of the catalog by Clement et al. (2001)[3] there are 90 variables in the field of M53. We have recovered the light curves of 64 of them. Out of 26 known variables which we could not recover, 12 were outside our FOV, 13 were saturated on our RF, and 1 was at the edge of the CCD. In Table 1, we list the obtained equatorial coordinates (J2000.0) of the known variables recovered in our study, their offsets to the coordinates given by Clement et al. (2001), and their Two Micron All Sky Survey (2MASS) identifications, if any. The offsets were calculated using

$$r'' = \arccos\left[\sin\delta_1 \sin\delta_2 \times \cos(\alpha_1 - \alpha_2) + \cos\delta_1 \times \cos\delta_2\right], \quad (1)$$

where (α_1, δ_1) and (α_2, δ_2) are the right ascensions and declinations of the stars for which the offset is to be calculated. We also provide the equatorial coordinates for variables from V61 to V70, which are not given in Clement's catalog. Several cases in Table 1 deserve special note and are described in the text.

3.1. Variable Stars with Periods $P > 0.1$ Days

Though we have obtained light curves for most of the previously detected variables in this period range, we would not like to make conclusions regarding their variability due to the short span of our observations. However, several stars in this period range deserve special mention.

3.1.1. Notes on Individual Variables

V33. Both Clement's (obtained from Evstigneeva et al. 1997) and our coordinates do not match the position of this variable as marked in the Kopacki (2000) ID chart. However, it is situated very close to the very bright secondary standard star S4 that is nearly saturated on our RF, which may account for the shift in the light centroid in our case.

V52–V53. These two stars are separated by ∼2″ and DK reported that they could not resolve them. However, V52 is clearly resolved on our images and its coordinates coincide with the coordinates given by Clement et al. (2001) with 0.″3 offset. Though we could not determine its period, its light curve shows RRlab-type variability. At the position of V53 given by Kopacki (2000), there are three stars, one of which does show some variability; however, its independent variability is questionable. The 2MASS position for V53 is between these three stars.

V57. The coordinates of the star identified by Kopacki (2000) as V57 do not match the coordinates given by Evstigneeva et al. (1997). The coordinates of Evstigneeva et al. (1997) match another, fainter star close to it. To investigate further, we have checked both stars, marked V57_1 and V57_2, respectively, for variability. The star identified by Kopacki as V57 (our V57_1) does not show any variability, though with the listed period of $P = 0.5683$ days, its light curve should have shown some variation over our 7.5 hr of observations, whereas the star that matches with Evstigneeva's coordinates (our V57_2) shows very clear variability with possible two pulsation periods of different amplitudes. Due to the limited time span of our observations, we could not determine its period, but the presence of the Blazhko effect can be suspected from the observed light curve. Thus, we conclude that the star identified and marked on the ID chart by Kopacki (2000) as V57 is a misidentification, and the correct coordinates are given in Evstigneeva et al. (1997). There is one more star within this field, marked as V57_3, which is also most probably not a genuine variable. In Figure 3, we show all three stars, marked accordingly, and their time-domain light curves. When we cross-correlated our list of known variables with the BSS catalog by Beccari et al. (2008; see Section 4.7), we found a match with BSS 102387 from the *Hubble Space Telescope*/WFPC2/PC sample to within 0.″6 (coordinates of that BSS are between these three stars, closer to a brighter V57_1). Since V57 was identified as an RR Lyrae previously (for example, see Kopacki 2000), it is possible that either V57_3 is a variable after all, or that Beccari et al. (2008) could not resolve these three stars and used their combined light to derive their conclusion. More work on this identification of this BSS is in progress.

V61–V70. For these stars, the updated 2010 online version of catalog by Clement et al. (2001) does not provide equatorial coordinates. We have determined the coordinates of all of these stars and matched them to the 2MASS catalog (Table 2). For V61, DK did not provide the light curve as they stated that this star is merged with the long-period variable (LPV) V49 on their images. However, it shall be noted that variable V49 (2MASS ID J13125915+1814356) is a star well outside the cluster core

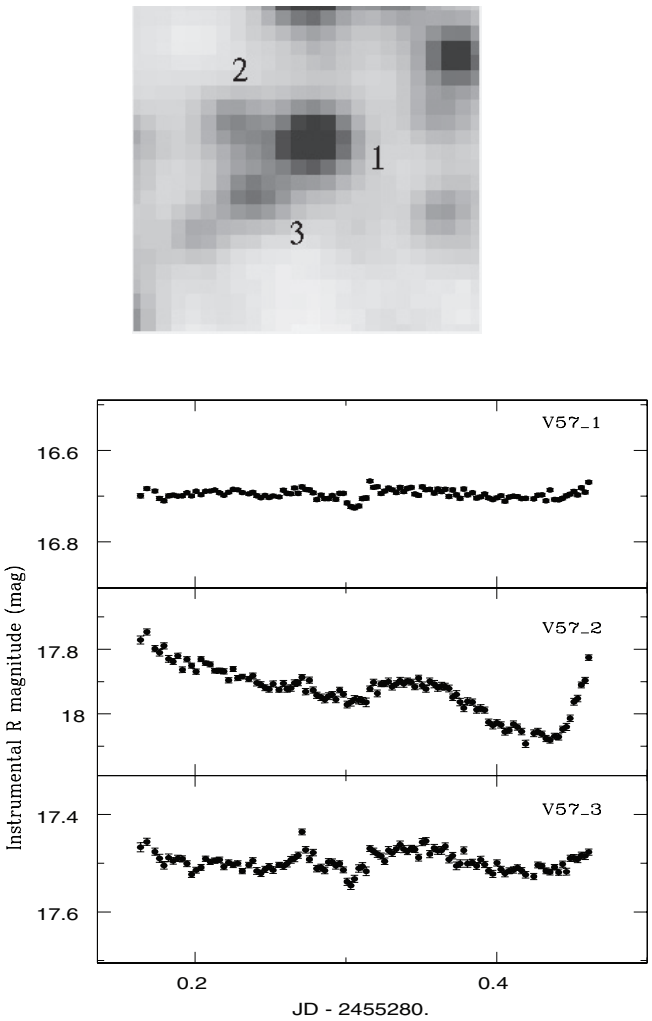

Figure 3. 7″ × 7″ field around V57 with marked stars and the light curves of V57_1, V57_2, and V57_3. The names of the stars are indicated on each panel.

[3] A full updatable catalog is accessible at http://www.astro.utoronto.ca/~cclement/cat/listngc.html.

Table 1
Revised Equatorial Coordinates of Identified Previously Known Variables in M53 and their Offsets with those given in the Catalog by Clement et al. (2001)

ID	α(2000) (h:m:s)	δ(2000) (° :′:″)	Offset (″)	2MASS ID	Notes/Remarks
V1	13:12:56.34	18:07:13.8	0.823	J13125634+1807139	
V2	13:12:50.27	18:07:00.8	0.511	J13125028+1807007	
V3	13:12:51.37	18:07:45.4	0.688	J13125132+1807461	
V4	13:12:43.88	18:07:26.2	0.559	J13124390+1807259	
V5	13:12:39.09	18:05:42.6	0.349	J13123907+1805424	
V6	13:13:03.90	18:10:20.1	0.541	J13130390+1810202	
V7	13:13:00.85	18:11:30.0	0.609	J13130086+1811302	
V8	13:13:00.42	18:11:05.1	0.615	J13130043+1811049	
V9	13:13:00.07	18:09:25.1	0.639	J13130013+1809256	
V10	13:12:45.72	18:10:55.5	0.467	J13124572+1810554	
V11	13:12:45.37	18:09:01.9	0.583	J13124540+1809020	
V15	13:13:12.374	18:13:55.6	0.500	...	
V16	13:12:46.19	18:06:39.1	0.541	J13124620+1806387	
V17	13:12:40.34	18:11:54.1	0.418	J13124030+1811540	
V18	13:12:48.67	18:10:13.1	0.590	J13124868+1810128	
V19	13:13:07.00	18:09:26.3	0.559	J13130702+1809262	
V22	13:12:51.97	18:05:16.7	0.327	J13125197+1805165	
V23	13:13:02.33	18:08:36.1	0.443	J13130235+1808359	
V24	13:12:47.28	18:09:32.3	0.566	...	
V25	13:13:04.40	18:10:37.3	0.664	J13130441+1810372	
V27	13:12:41.42	18:07:23.7	0.541	J13124143+1807235	
V29	13:13:04.26	18:08:47.0	0.443	J13130426+1808468	
V31	13:12:59.56	18:10:04.9	0.535	J13125960+1810046	
V32	13:12:47.72	18:08:35.8	0.488	J13124774+1808358	
V33	13:12:43.89	18:10:12.1	1.416	...	See individual notes
V34	13:12:45.70	18:06:26.0	0.566	J13124569+1806258	
V35	13:13:02.41	18:12:37.9	0.464	J13130235+1812373	
V36	13:13:03.28	18:15:10.5	0.535	J13130329+1815109	
V37	13:12:52.28	18:11:05.3	0.492	J13125227+1811050	
V38	13:12:57.14	18:07:40.5	0.727	J13125713+1807404	
V39	13:12:38.74	18:13:31.3	0.516	J13123874+1813312	
V40	13:12:55.85	18:11:54.8	0.535	J13125583+1811545	
V41	13:12:56.75	18:11:08.5	0.630	J13125679+1811093	
V42	13:12:50.55	18:10:20.0	0.395	J13125058+1810195	
V43	13:12:53.08	18:10:55.4	0.511	J13125306+1810552	
V44	13:12:51.66	18:10:00.5	0.590	...	
V45	13:12:55.15	18:09:27.4	0.590	J13125517+1809274	
V46	13:12:54.53	18:10:37.1	0.418	...	
V47	13:12:50.41	18:12:24.7	0.492	J13125043+1812246	
V51	13:12:57.58	18:10:49.6	0.549	...	
V52	13:12:55.91	18:10:37.0	0.327	...	See individual notes
V53	13:12:55.78	18:10:36.0	0.615	J13125580+1810360	See individual notes
V54	13:12:54.29	18:10:31.5	0.590	...	
V55	13:12:53.45	18:10:36.6	0.492	...	
V56	13:12:53.69	18:09:26.0	0.590	...	
V57	13:12:55.55	18:09:58.6	0.418	J13125547+1809577	BSS match, see individual notes
V58	13:12:55.59	18:09:31.0	0.492	...	
V59	13:12:56.67	18:09:20.8	0.441	...	
V60	13:12:56.99	18:09:36.5	0.418	J13125695+1809357	
V61–V70					See individual notes
V72	13:12:55.942	18:09:52.12	2.522	...	See individual notes
V73	13:13:03.34	18:09:25.1	0.655	...	
V74	13:12:49.68	18:07:25.9	0.427	...	BSS, Beccari et al. (2008)
V75	13:13:09.39	18:09:39.7	0.792	...	BSS, first report
V76	13:13:04.97	18:08:35.8	0.658	...	BSS, Beccari et al. (2008)
V79	13:12:46.60	18:11:36.7	0.148	...	BSS, report by DK
V80	13:12:57.46	18:10:14.8	1.294	...	See individual notes
V81	13:13:02.69	18:06:29.7	0.283	J13130271+1806294	
V82	13:12:56.44	18:13:09.9	0.850	...	
V83	13:12:50.11	18:07:43.0	0.187	...	
V87	13:13:01.92	18:10:13.2	0.475	...	BSS, first report
V89	13:13:08.15	18:07:38.4	0.884	...	BSS, first report

Notes. In the catalog by Clement et al. (2001), the coordinates for the above variables are compiled from different sources. Coordinates for variables numbered up to V60 are from Evstigneeva et al. (1997); V71–V72 and V77–V86 from DK; and for V73–V76, V87, and V89 from Jeon et al. (2003). For variables V61–V70, Clement et al. (2001) provide only X and Y coordinates.

Table 2
Equatorial Coordinates (α, δ) of Known Variables V61–V70

ID	α(2000) (h:m:s)	δ(2000) (° :′:″)	2MASS ID (J2000.0)	Note
V61	13:12:55.214	18:10:10.31	J13125521+1810103	
V62	13:12:53.995	18:10:29.81	J13125400+1810302	
V63	13:12:56.300	18:10:00.75	...	
V64	13:12:52.515	18:10:12.54	J13125254+1810125	
V65	13:13:04.669	18:10:59.44	J13130467+1810594	≡S67
V66	13:13:01.578	18:10:03.90	J13130157+1810039	
V67	13:13:01.024	18:10:09.50	J13130102+1810095	
V68	13:12:56.577	18:08:23.13	J13125657+1808231	
V69	13:12:55.160	18:10:19.40	J13125616+1810194	
V70	13:12:55.320	18:09:42.00	J13125532+1809420	

Table 3
Revised Periods for Previously Known Short-period Variables in M53

ID	Period (days)	New Period (days)	$\langle R \rangle$ (mag)	Note
V73	0.0701	0.071530	18.927	
V74	0.0454	0.045055	19.054	BSS
V75	0.0442	0.044178	19.455	BSS
V76	0.0415	0.041467	19.434	BSS
V79	0.0463	0.046255	19.183	BSS
V80	0.0674	0.065668	17.915	See individual notes
V81	0.0714	NV	17.310	See individual notes
V82	0.0221	NV	18.864	See individual notes
V83	0.1247	NV	18.749	See individual notes
V87	0.0479	0.046855	19.356	BSS
V89	0.0435	0.43278	19.435	BSS

Notes. Column 1 is the star's ID from the Clement et al. (2001) nomenclature, Column 2—periods from the literature, Columns 3 and 4—new periods and standard R magnitudes found in this work. Periods in the second column are from DK, except for stars V87 and V89 where periods are from Jeon et al. (2003). NV stands for non-variable and BSS means that the star belongs to the BSS population.

at a distance of 4.′54 from the cluster center, while V61 is well inside the core at only 1.″8 from the center; thus, there is some mistake in their identification.

We shall note that for variables V62, V63, and V64, three sets of coordinates are available: from the online catalog by Samus et al. (2009),[4] derived from the 2MASS catalog (probably precessed from J2000.0 to J2000.343), DK's, and ours. For V62, Samus et al. (2009) give a position between V62 and a star to the north from it with 0.″535 offset, while DK's and our coordinates coincide within 0.″12 with its position. V63 has no 2MASS match; Samus et al.'s (2009) and our coordinates match within 0.″02, but DK's coordinates are off by 2.″44 and actually mark a different, non-varying star. For V64, Samus et al. (2009) use 2MASS coordinates (at J2000.343 epoch), but these give a position shifted by 0.″374 to the left, and DK miss the position by 1.″215. The remaining variables, V65 to V70, match perfectly with 2MASS sources. V65 is the Stetson (2000) secondary standard star S67 (see Section 3.3).

V72. We did not find any variability of the star that matches the coordinates given by DK. Though V72 is situated in the heavily crowded core, we have clearly identified five stars within a 2.″75 radius of the coordinates given by DK. The star which is variable according to DK is marked as V72_1, the rest as V72_2, V72_3, V72_4, and V72_5, respectively. While four of them do not show obvious variability, the star V72_2 is clearly varying with an estimated period of ∼0.295 days and an amplitude of ∼$0^{m}.195$ (these values were obtained by the IRAF phase-dispersion minimization (pdm) task). We conclude that it is the star V72 identified by DK. The coordinates of V72_2 and its offset from DK coordinates are given in Table 1. In Figure 4, we show the 6.″5 × 6.″5 field around the coordinates given by DK, phase plot of V72_2, and time-domain light curves of these two stars.

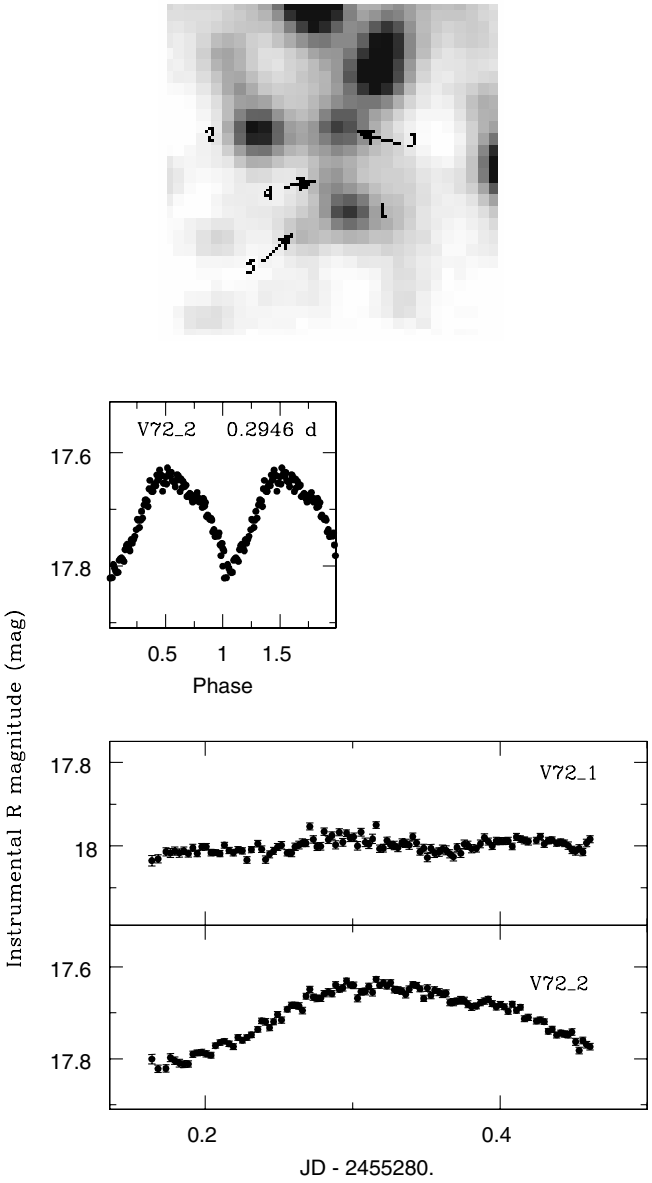

Figure 4. 6.″5 × 6.″5 field around the V72 position as given by DK with marked stars, phase plot of V72_2, and light curves of V72_1 and V72_2 stars.

3.2. Variables with Periods $P < 0.1$ Days

There are 15 SPV stars of SX Phe type reported so far in M53. From our observations we were able to recover 11 of those stars. Three stars, V77, V88, and V90, were out of our FOV and one, V78, was saturated on our RF. For these 11 stars, we have obtained the light curves and determined the periods. In several cases we have revised the periods given previously

[4] The full catalog is available at http://vizier.cfa.harvard.edu/viz-bin/VizieR?-source=J/PASP/121/1378. However, there is a mistake in the online catalog star listing—the coordinates of a variable V46 are lost; instead the coordinates of V47 are assigned to it, and this mistake carries on until the end of the catalog.

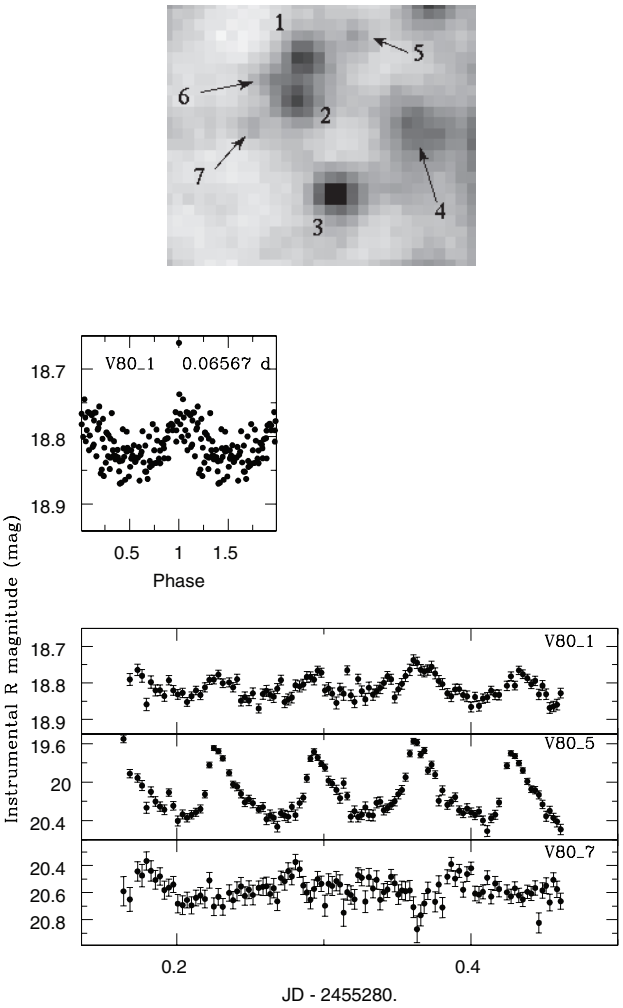

Figure 5. 6.″5 × 6.″5 field around V80 with marked stars, phase plot of V80_1, and light curves of the V80_1, V80_5, and V80_7 stars.

in the literature. In Table 3, we list these stars along with the previously reported periods, new periods, and the average *R*-band magnitudes determined in this work.

V80. At the coordinates given by DK, there is no star. However, within a circle of radius 3.″184 on this location there are seven stars clearly seen on our RF. This image region is shown in Figure 5 with the seven stars marked on it. We have run the periodicity check (see details in Section 4.3) on the light curves of all of these stars. Three of them, V80_1, V80_5, and V80_7, show short-term variability and their light curves are shown in Figure 5. Of these, V80_1 and V80_5 show similar light curves and periods characteristic of SX Phe stars, but V80_5 has a much larger variation amplitude of $\Delta m = 0.9$ compared with $\Delta m = 0.2$ of V80_1. The light curve of the variable V80_7 is noisy with an amplitude of $\Delta m \approx 0.6$. It shall be noted that DK could not have determined the exact position of V80 as they reported that this particular field was heavily crowded or blended on their RF. By comparing the light curves of their V80 and our candidates, we conclude that the most probable match is candidate V80_1 (it has the same symmetric sinusoidal curve). The other two candidates, V80_5 and V80_7, thus constitute new variables. Details on V80_5 are presented in Table 6, where it is assigned the name SX25, and on V80_7 in Table 9.

V81, V82, V83. These three stars were first reported by DK as SX Phe stars. V81 star is clearly resolved on our RF and has a

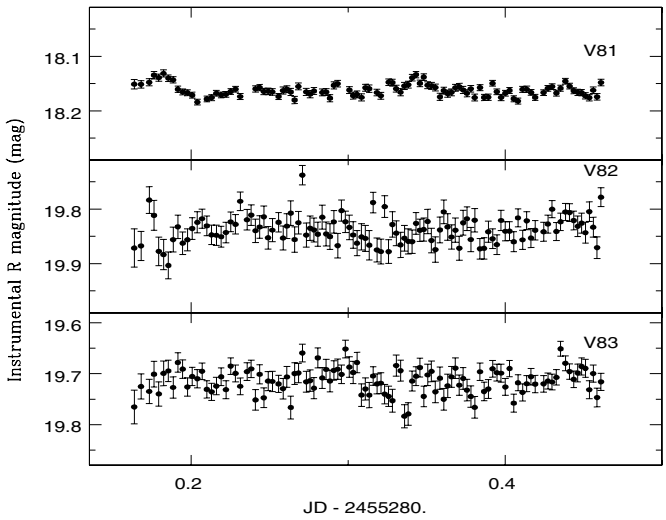

Figure 6. Light curves of the V81, V82, and V83 stars.

Table 4
Results of the Variability Criteria for Stars V81, V82, and V83

ID	$\mathcal{A}$	$\mathcal{F}$	rms	σ_{XS}
V81	2.7	5.08×10^{-3}	0.01123	0.05233
V82	−0.063	7.85×10^{-2}	0.0255	0.0751
V83	0.235	8.42×10^{-1}	0.0254	0.0844

Notes. $\mathcal{A}$ is the alarm statistics, $\mathcal{F}$ is the significance level of periodicity found, rms is the standard deviation of the mean instrumental magnitude, and σ_{XS} is the excess variance.

2MASS match. However, we find it non-variable. DK reported that its variability is either of unknown type or that it was blended with a nearby suspected BSS, identified by them with USNO star B1.0 1081-0245846. However, USNO coordinates are located between V81 and two nearby faint stars that do not show any variability. Stars V82 and V83 are also clearly resolved on our RF and also do not show variability of the type reported by DK (see the light curves in Figure 6). The results of the variability criteria (details are in Section 4.4) shown in Table 4 also indicate that these three stars are most probably not variable.

3.3. Variability in Standards

Out of 192 photometric standard stars known in M53, we have selected 46 for our astrometric calibration (Section 2.4). However, when we tried to use these stars to devise the variable search criteria, some of the selected standard stars were picked up as variable by our selection criteria (see Table 5). This fact by itself is not very unusual, as this is not the first time when standard stars in this cluster are found to be variable. Two variables discovered by DK, namely V84 and V85, and identified by them as LPV with periods of 22.4 and 19.8 days, respectively, are in fact Stetson's standard stars S1 and S17 (Stetson 2000). One more variable star, V65, identified by Kopacki (2000) as SR type, although he could not determine its period, is again the standard star S67 (Stetson 2000). We could not confirm their variability as all three stars were saturated on our RF, but we report this fact for the first time to our knowledge.

We have examined our selected standards for variability by eye. We noticed that several stars (Table 5 and Figure 7) exhibit nearly identical variability of the type previously discussed in Section 2.3 and displayed in Figure 2, and have concluded that this is the result of spurious, or induced, variability due to

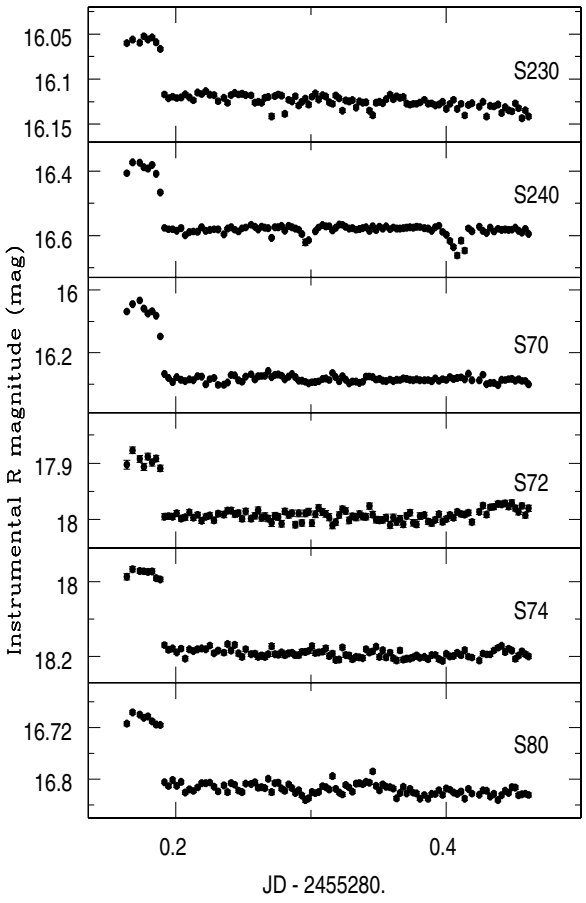

Figure 7. Light curves of standards suspected as variable.

the combination of the intra-night PSF changes and DanDIA reduction procedure (see Section 2.3). It was important to recognize this type of variability as spurious and that is why all our candidate variables had to be inspected by eye, since these standards were passed by our variability criteria (Section 4.4) as variable. In Table 5, we give the details of their variability statistics. It is interesting to note that star S240, apart from obviously induced variability, displays the possible signature of an EA-type[5] eclipsing binary light curve. However, to determine the true light curve, this star has to be examined in greater detail. This will be done in a separate study.

4. DETECTION OF NEW VARIABLES

The primary goal of our main survey is to identify possible ML events. We have used the commissioning data set to tune up and test our data reduction and analysis pipeline on variability search. We would expect to find false positives in the ML search—variable stars like dwarf novae, classic novae, etc., that can be confused with genuine ML events (see Safonova & Stalin 2010 for a discussion on contamination of ML searches). Finding these events and successfully identifying them would demonstrate our ability to detect actual ML events in our data set in the future. The search can also yield interesting variable stars not found through earlier variable selection methods.

Due to the large numbers, it is necessary to automate the detection of variable sources. To search the data set of ~10,000 light curves for variable stars, we employ several methods as we found that no single algorithm is appropriate for the detection of all kinds of variability and that false positives (or missing variables) are high if we use just one algorithm. We thus devised a combined criterion to select promising candidates. In addition, we only considered light curves with more than 60 data points, since several variability detection algorithms can produce incorrect results when a significant amount of data is missing.

[5] According to the new globular clusters variable star (GCVS) catalog classification, EA stands for Algol-type detached eclipsing binary.

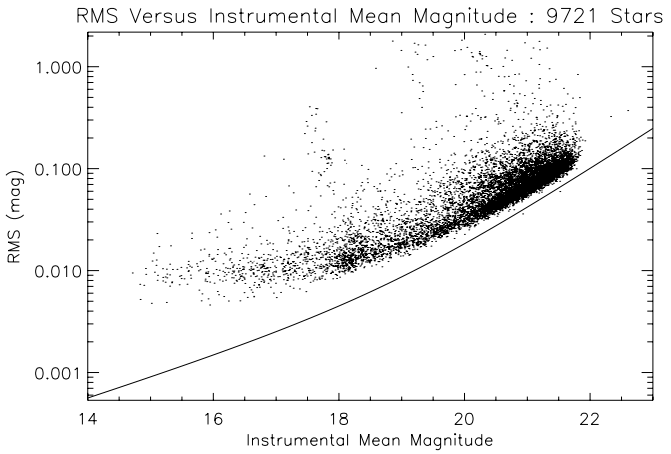

Figure 8. Plot of rms vs. mean instrumental r magnitude for each of the 9721 light curves. The solid line shows the theoretical limits (photon noise).

Table 5
Some of the Standards from Stetson's Catalog (Stetson 2000) that Exhibited Spurious Variability During our Observational Run

ID	$\langle R\rangle$(mag)	Δr(mag)	rms	$\mathcal{F}$	$\mathcal{A}$	$\sigma_{\rm XS}$
S70	15.562	0.269	0.057	4.4×10^{-4}	6.78	0.35
S72	17.151	0.133	0.027	1.7×10^{-5}	6.43	0.147
S74	17.327	0.244	0.057	3.5×10^{-5}	6.73	0.31
S80	16.061	0.136	0.029	1.2×10^{-5}	8.31	0.175
S230	15.425	0.091	0.019	1.1×10^{-7}	8.34	0.116
S240	15.841	0.289	0.052	7.7×10^{-4}	7.32	0.31

Notes. Column 1 is the star's ID in Stetson (2000), Columns 2 and 3 are the mean standard R magnitudes and range of observed variation. Columns 4–7 are the computed variability statistics (Section 4.4): rms is the standard deviation of the mean instrumental magnitude, $\mathcal{F}$ is the significance level of periodicity, $\mathcal{A}$ is the alarm statistics, and $\sigma_{\rm XS}$ is the excess variance.

4.1. Alarm Statistics

As a first algorithm, we have selected the alarm statistics from the VARTOOLS software package (Hartman et al. 2008). The "alarm" $\mathcal{A}$ is defined as (Tamuz et al. 2006)

$$\mathcal{A} = \frac{1}{\chi^2}\sum_{i=1}^{K}\left(\frac{r_{i,1}}{\sigma_{i,1}}+\frac{r_{i,2}}{\sigma_{i,2}}+\ldots+\frac{r_{i,k_i}}{\sigma_{i,k_i}}\right)^2-\left(1+\frac{4}{\pi}\right), \quad (2)$$

where k_i is the number of residuals in the ith run, $r_{i,j}$ is the residual of the jth measurement of the ith run, and $\sigma_{i,j}$ is its uncertainty. The sum is over all the measurements in a run and then over the K runs, where a "run" is defined as a maximal series of consecutive residuals with the same sign in the phased light curve. The χ^2 is the usual function

$$\chi^2 = \sum_{i=1}^{N}\left(\frac{r_i}{\sigma_i}\right)^2, \quad (3)$$

Table 6
Equatorial Coordinates and Light Curve Parameters for SX-Phe-type Candidates in M53

Variable Designation	α(2000) (h:m:s)	δ(2000) (° :′:″)	P (d)	$\langle R \rangle$ (mag)	Δr (mag)	Epoch (d)	Note
SX2	13:12:48.29	18:13:18.7	0.039362	19.6018	0.2924	0.2039	SX Phe,F,BSS
SX3	13:12:48.27	18:14:34.5	0.059824	18.7855	0.16501	0.1763	SX Phe,F,BSS
SX4	13:12:48.69	18:10:10.2	0.049500	19.4494	0.41865	0.3733	SX Phe,F,BSS
SX6	13:12:49.91	18:08:56.5	0.044755	18.1171	0.16693	0.3482	SX Phe,H,BSS
SX7	13:12:51.74	18:10:33.8	0.132701	19.6519	0.37991	0.2409	Not SX Phe, uncertain
SX8	13:12:52.03	18:09:53.6	0.099101	18.7416	0.37707	0.2517	SX Phe,F
SX9_1[a]	13:12:52.91	18:10:35.7	0.054056	18.5738	0.2819	0.216	SX Phe,BSS?
SX9[a]	13:12:52.99	18:10:35.4	0.056756	19.6975	0.59367	0.216	BSS?
SX11	13:12:53.66	18:08:57.7	0.052932	19.3140	0.42881	0.2807	SX Phe,F
SX12	13:12:53.89	18:09:13.2	0.100001	19.4074	0.32196	0.3807	Not SX Phe, uncertain
SX13	13:12:54.52	18:09:32.6	0.112712	19.4671	0.49331	0.3733	Not SX Phe, uncertain
SX14	13:12:54.78	18:09:37.6	0.071130	18.6844	0.52035	0.3032	SX Phe,F,BSS
SX15	13:12:56.34	18:11:54.2	0.137101	20.4167	0.60844	0.3258	Not SX Phe, uncertain
SX16	13:12:56.37	18:11:05.4	0.049900	17.9848	0.17625	0.1637	SX Phe,H
SX17	13:12:57.17	18:09:41.9	0.040567	18.0077	0.13385	0.1824	SX Phe,H,BSS
SX24	13:12:57.64	18:10:43.0	0.033724	18.4832	0.16544	0.3733	SX Phe,H
SX19	13:12:58.30	18:08:41.3	0.044378	19.3035	0.33948	0.1637	SX Phe,F,BSS
SX20	13:12:59.53	18:09:17.5	0.134857	18.7493	0.16805	0.384	Not SX Phe, uncertain
SX21	13:12:59.51	18:11:17.4	0.037762	19.5682	0.26318	0.2983	SX Phe,F,BSS
SX22	13:13:01.92	18:12:30.4	0.045955	19.5604	0.38023	0.1824	SX Phe,F
SX23	13:13:04.21	18:10:59.4	0.107312	19.6818	0.38479	0.2039	Not SX Phe, uncertain
SX25	13:12:57.37	18:10:15.3	0.066868	19.1302	0.96035	0.4111	≡V80_5,SX Phe,F

Notes. Δr and epoch were obtained by IRAF task pdm.
[a] These two stars are separated by 1.″2. Though their periods and epochs are nearly the same, which could support the argument that there is only one variable, the amplitude of a fainter star is twice that of a brighter star. They also match within 1″ to a BSS (see Section 4.7), the coordinates of which (Beccari et al. 2008) are located exactly between these two stars. More discussion is in the text.

and the sum is over N observations. The minimal value of the summation in Equation (2) is exactly χ^2, and thus the minimal value of $\mathcal{A}$ is $-4/\pi$. It is minimal when the residuals alternate between positive and negative values, while long runs with large residuals increase its value. We find that as an initial assessment, the alarm statistics is good for large sudden (aperiodic) variations, but that it fails in the case of the short-period variability. It cannot easily distinguish between non-variability with large noise and very regular short periodicity, which we already noticed when we tried to use the ordinary χ^2-statistics. In contrast to χ^2 itself, $\mathcal{A}$ is not sensitive to a systematic overestimation or underestimation of the uncertainties. However, even in detecting large variations, the alarm results have to be viewed with caution, as it may pick up the false variability, as in the case of systematic variations found in standard stars (see Section 3.3). We still found it useful, as high values of alarm statistics may indicate an eclipsing binary, ML event, or any non-periodic transient.

4.2. Excess Variance

The light curve of a variable star candidate has variations due to measurement errors σ_i and intrinsic variations. The variance of such a light curve consisting of N data points with amplitude X_i is given by

$$S^2 = \frac{1}{N-1} \sum_{i=1}^{N} (X_i - \langle X \rangle)^2 \ . \tag{4}$$

This measured S^2 has contributions from both intrinsic source variability and measurement uncertainty. Therefore, to know if any intrinsic variations are present in the light curve, any contribution of the measurement errors to the observed variance needs to be removed. A commonly used approach to evaluate the intrinsic variation present in the candidate light curve is the "excess variance" method (Nandra et al. 1997; Vaughan et al. 2003), where excess variance is defined as

$$\sigma_{\rm XS}^2 = S^2 - \sigma_{\rm err}^2 \, , \tag{5}$$

where $\sigma_{\rm err}^2$ is the average variance of the N measurements, given as

$$\langle \sigma_{\rm err}^2 \rangle = \frac{1}{N} \sum_{i=1}^{N} \sigma_{{\rm err},i}^2 \, . \tag{6}$$

A large value of $\sigma_{\rm XS}^2$, much in excess of the measurement errors, indicates the presence of variations in the light curve.

4.3. Lomb–Scargle Periodogram

The Lomb–Scargle (LS) periodogram (Lomb 1976) is an algorithm designed to pick out periodic variation in an unevenly sampled data. The periodogram statistic, Θ, is the measure for the fit at a given pulsation frequency. Its probability distribution is used to calculate the probability, $P(\Theta > c)$, of obtaining the value of the periodogram higher than the actual observed value, $\Theta = c$, from a hypothetical pure noise signal. An unlikely good fit, corresponding to small probability, is interpreted as detection of the corresponding period. The complement probability, $\mathcal{F} = 1 - P(\Theta > c)$, is called the significance level, because it estimates the significance of the height of a peak in the periodogram. Thus, the likelihood of the existence of a periodic signal can be established with $\mathcal{F}$, where the smaller the value of $\mathcal{F}$, the higher the significance of the detected periodicity. We have used the implementation of this algorithm given in Press et al. (1992, p. 569) and this seems to be a good method for detecting periodic variability present in the data set.

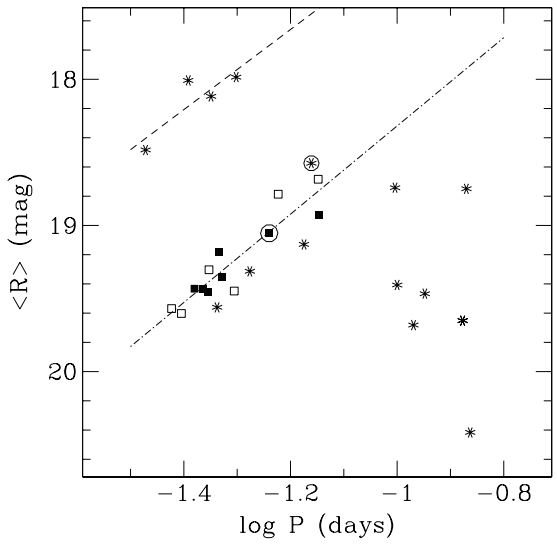

Figure 9. Mean R magnitude vs. period diagram. Squares represent stars used in the fundamental mode fitting; filled squares are previously known SX Phe stars in M53 and open squares are new SX Phe. The encircled filled square is the star V74 with the period converted from first harmonic to fundamental mode. Asterisks are the remaining SX Phe candidates. The encircled asterisk is the SX Phe candidate SX9_1 with the period converted to fundamental mode. The four asterisks at the top are most probably SX Phe in a higher pulsation mode and we have derived the linear fit for them.

4.4. Final Selection

To select candidate variable stars from the original light curve database, we used a combination of the three algorithms described above, namely (1) alarm statistics, (2) excess variance, and (3) the Lomb periodogram, together with the usual rms scatter estimate. The rms frame-to-frame scatter of the instrumental magnitude is a good indicator of the accuracy of the photometry. In addition, stars with a large dispersion for a given magnitude are, in principle, good variable candidates. However, it is possible that a light curve has a large rms due to bad measurements in some images, in which case the variability is spurious. Figure 8 shows the rms as a function of the mean instrumental magnitude for all light curves.

After applying these methods to the sets of secondary photometric standards and previously known variable stars in M53 (total of 114 stars), we have devised the following combined criterion for the final selection of variables from our list of ∼9700 candidate variable stars,

$$\begin{cases} \mathcal{A} > 1.0\,; \\ \mathcal{F} < 10^{-4}\,; \\ \sigma_{\rm XS} > 0.09\,; \\ {\rm rms} > 0.01\,. \end{cases} \qquad (7)$$

A total of 310 candidate variable stars were found to satisfy the criterion simultaneously. For these candidates, we calculated the periods using two methods: the Lomb periodogram (LS) and the algorithm of Lafler & Kinman (1965, hereafter LK). From the highest peak in the Lomb periodogram, we take the initial estimate of the period and pass it on to the LK algorithm. The LK method tests a series of trial periods (with an increment of 0.0001 days) and looks for the period that results in the "smoothest" phase curve. In this method, the N observed points are sorted by phase, and the sum of the squares of the difference in magnitude of successive pairs of points is used to rank the trial period. The smallest value of the figure of merit here is

$$\Theta = \sum_i (m_i - m_{i+1}) \Big/ \sum_i (m_i - \overline{M})^2\,, \qquad (8)$$

where $\overline{M} = m_i/N$ should be nearest to the correct period since this represents the smallest successive changes in the light curve.

Table 7
Equatorial Coordinates and Light Curve Parameters for New Suspected RR-Lyrae-type Stars in M53

Variable Designation	α(2000) (h:m:s)	δ(2000) (° :′″:)	$\langle R\rangle$ (mag)	Remarks
RR1	13:12:45.40	18:09:04.1	19.862	RRab
RR2	13:12:48.74	18:10:12.7	19.567	RRab
RR3	13:12:53.82	18:09:18.7	18.154	RRc
RR4	13:12:54.03	18:09:11.4	19.092	RRc
RR5	13:13:01.33	18:10:15.9	19.686	RRc
RR6	13:12:47.13	18:10:29.0	20.209	RRc?
RR7	13:12:54.58	18:09:45.4	18.076	RRc?
RR8	13:12:56.18	18:11:55.6	18.748	RRc
RR9	13:12:58.51	18:10:41.3	19.848	RRc?
RR10	13:12:58.38	18:09:59.5	18.560	RRab?
RR11	13:12:57.23	18:11:02.3	18.794	RRc
RR12	13:12:56.51	18:07:16.0	19.829	RRc
RR13	13:12:56.33	18:10:56.3	19.166	RRab
RR14	13:12:55.52	18:09:36.9	19.092	RRc

4.5. False Positives

Finally, we visually inspect the light curves to remove false positives. We noticed that due to the intra-night changes of the PSF, several stars selected as variables by our selection criteria have, in fact, variability induced by the same mechanism discussed in Section 2.3. This type of variability is easily detected by eye as it is virtually identical in such false light curves, and these stars were removed from the candidate list. We also noted that during our continuous observations for ∼7.5 hr, the coordinates of the field center drift between the images through the night. The typical intra-night drift was ∼25 pixels, but it had some effects in our data. The drift caused stars at the edges of the field to enter and exit the CCD's FOV during the night, resulting in incomplete light curves for those stars. We remedied that by eliminating strips of ∼20 pixel width along the edges of our images. Finally, we reject any variable star that is less than 10 pixels away from a variable candidate and has higher rms in flux. This criterion enabled us to eliminate stars whose variability was induced by its proximity to a genuine variable.

4.6. The Classification of New Variables

The precision of the relative photometry allowed us to definitely establish the fact of light variations in the variable star candidates. However, the total duration of our observations was not long enough for reliable classification of a large number of them. Nevertheless, the obtained light curves made it possible to tentatively estimate the type of some of the discovered variables based on calculated periods, shapes, and characteristic features of the light curves.

4.6.1. Candidate SX-Phe-type Stars

We have found 21 stars whose light curve parameters, i.e., short-period characteristic shapes, allow us to classify them as

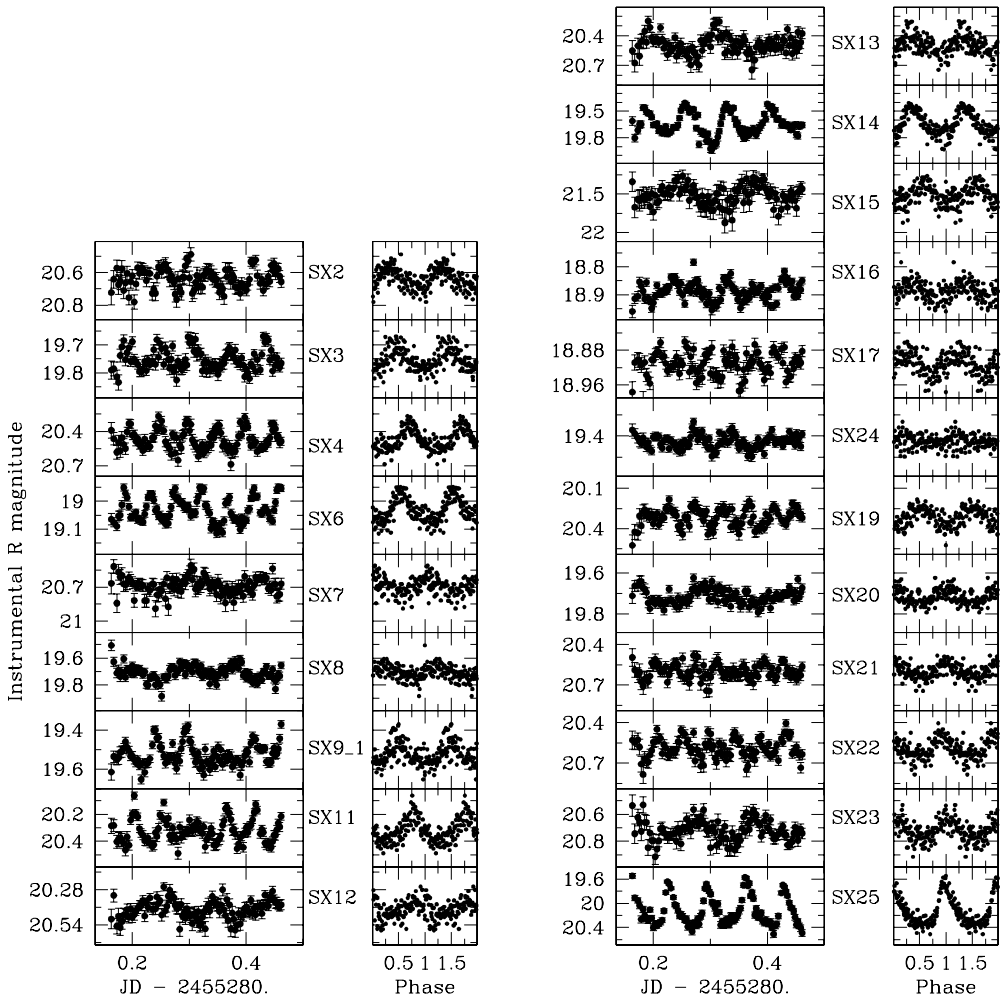

Figure 10. Phased and time-domain light curves of 21 SX Phe candidates from Table 6.

Table 8
Equatorial Coordinates and Light Curve Parameters for New Candidate Eclipsing Binaries in M53

Variable Designation	α(2000) (h:m:s)	δ(2000) (° :′″:)	Period (d)	$\langle R \rangle$ (mag)	Δr (mag)	Epoch (d)	Remarks
W1	13:12:43.70	18:10:09.0	0.095901	19.495	0.79939	0.1824	EW?
W2	13:12:51.07	18:11:11.9	0.146901	20.522	1.22333	0.3258	EW?
W3	13:12:51.41	18:09:37.4	0.155458	19.846	0.4898	0.2807	EW?
W4	13:12:53.98	18:09:49.0	0.102701	19.339	0.7531	0.3683	EW?
W5	13:12:53.21	18:09:47.3	0.130457	18.520	0.29791	0.3032	EW?
W6	13:12:57.46	18:10:29.6	0.090300	19.641	0.60217	0.3085	EW?
W8	13:12:56.66	18:08:18.7	0.108612	19.999	0.97774	0.3032	EW?
W9	13:12:59.00	18:10:21.9	0.151258	19.369	0.39071	0.3282	BSS, AH Vir?
W11	13:13:01.04	18:10:01.6	0.162858	19.881	0.53721	0.311	EW?
W13	13:13:11.43	18:10:34.2	0.120201	20.383	1.05576	0.1763	EW?

Notes. Δr and epoch were obtained by the IRAF task pdm. The quoted periods represent half the orbital period of the system. They are only approximate due to the short span of our observations.

potential SX Phe stars. SX Phe stars known in GCs usually have periods between 0.03 and 0.14 days and often show multiple frequencies of light variations. However, with our limited span of observations, it was very difficult to establish the complicated frequency patterns, so we aimed to find at least the main periodicity. The parameters of these candidates are listed in Table 6. For each star we provide designation, equatorial coordinates (α, δ), period P, mean brightness in R, range of variability Δr, epoch of light-minimum T = JD − 2,455,280 and in the Notes we present the BSS match, possible variability type, or pulsation mode as inferred from the P–L diagram (F stands for fundamental mode and H stands for higher pulsation mode).

Several methods are available to confirm the exact nature SX Phe candidates. It is known that observational identification of the pulsation modes in SX Phe is difficult. McNamara (2000),

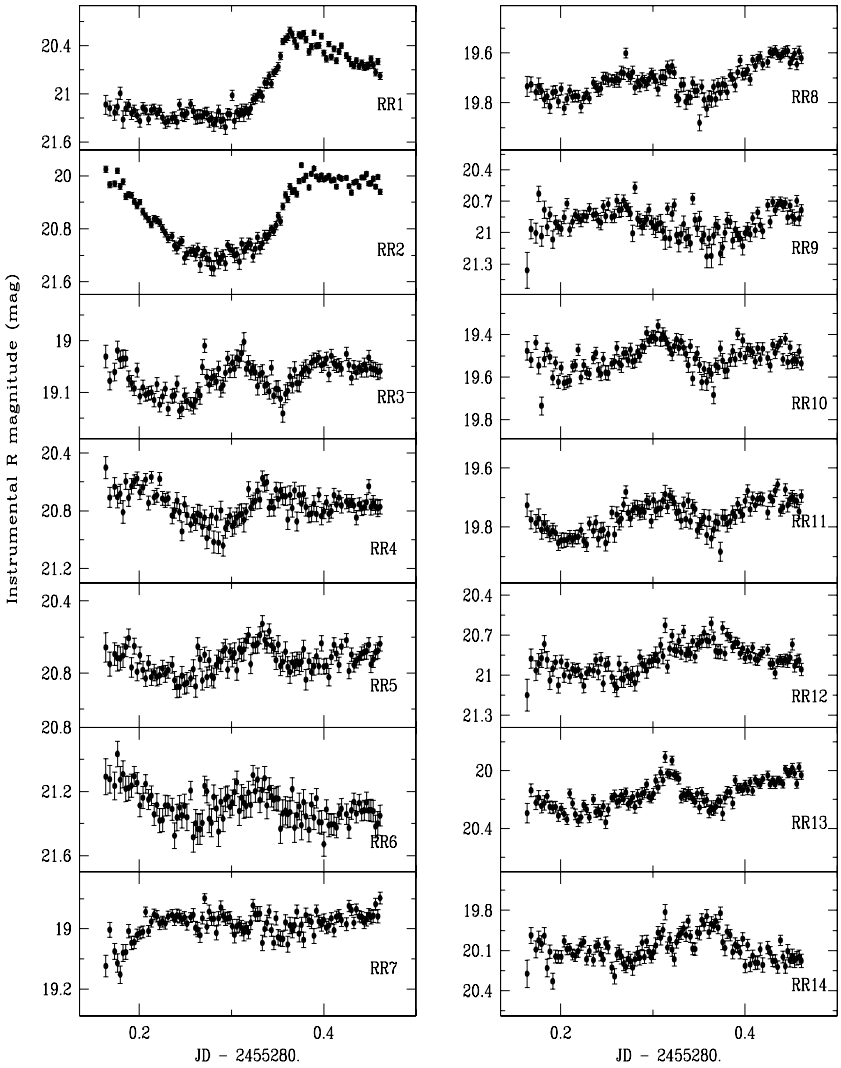

Figure 11. Time-domain light curves of RR Lyrae candidates.

and, subsequently, Rodríguez & López-González (2000), suggested that at fundamental mode, SX Phe stars preferably show large amplitudes (>0.2) and asymmetric light curves. They also follow a tight relation between their fundamental and first overtone mode periods and luminosity (P−L relation). SX Phe are also the BSSs that are found in a large number in GCs (∼200 in this cluster; Beccari et al. 2008). Thus, a match between known BSS and our SX Phe candidates would argue in favor of their SX Phe nature (see Section 4.7).

Based on a study of six SX Phe stars in M53, Jeon et al. (2003) derived the following P−L relation for the fundamental mode:

$$\langle V\rangle = -3.01(\pm 0.262)\log P + 15.31(\pm 0.048)\,. \quad (9)$$

We have used our derived periods and R magnitudes for seven previously known SX Phe stars (V73, V74, V75, V76, V87, and V89 from Jeon et al. 2003 and V79 from DK) and six new SX Phe candidates that have BSS matches (except SX9, SX9_1, SX6, and SX17; see the discussion later in this subsection) to derive the P−L relation. Our relation is surprisingly nearly identical to that of Jeon et al. (2003):

$$\langle R\rangle = -3.019(\pm 0.382)\log P + 15.300(\pm 0.501)\,. \quad (10)$$

In Figure 9, we display the period and mean R magnitude relation for 7 known SX Phe stars and 21 new SX Phe candidates in M53. We note that variable V74 was found by Jeon et al. (2003) to lie far away from the P−L line; this is possibly due to the wrong period reported by the authors in their Figure 7. Besides, the authors excluded this variable from the fundamental P−L fitting, suggesting that it was in a higher pulsation mode. However, if it is in the first harmonic mode, its period can be converted to the fundamental mode by the theoretical relation $P_{1H}/P_F = 0.783$ (Jeon et al. 2004). Once corrected for that, we can see that V74 lies on the P−L line together with other SX Phe stars (see Figure 9). In our sample of SX Phe candidates, we have two stars which have similar periods but different magnitudes (variables SX9_1 and SX_9 in Table 6). It is possible that only one of them is variable and another has variability induced by its proximity. Using the selection criteria adopted in Section 4.5, we choose the star that has smaller rms in flux to be genuinely variable; thus, we select the star SX9_1. This star lies above the fundamental mode P−L line; when we convert its period by using the same relation $P_{1H}/P_F = 0.783$ (Jeon et al. 2004), it falls close to that line. Stars with converted periods, SX9_1 and V74, are marked by circles in Figure 9.

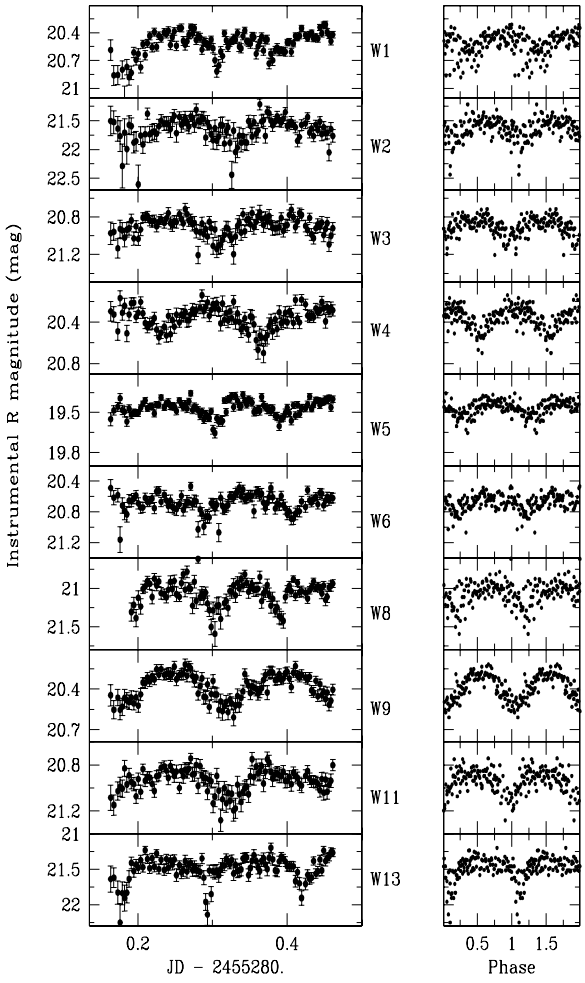

Figure 12. Phase and time-domain light curves of W UMa candidates.

The stars that fall along the $P-L$ relation can be considered with high probability, given also their periods and shape of light curves, as belonging to the SX Phe type. Stars in the top left quadrant of the plot (variables SX6, SX16, SX17, SX24) are presumably in a higher pulsation mode. They also have smaller amplitudes (0.1606 on average) compared to the ones pulsating presumably in fundamental mode (0.4365 on average). We have derived the least-squares fit for them and found that it is nearly parallel to the fundamental mode fit,

$$\langle R\rangle = -2.740(\pm 1.160)\log P + 14.371(\pm 1.600)\,. \qquad (11)$$

Stars SX7, SX20, SX12, SX13, SX15, and SX23, located to the right and below the fundamental $P-L$ line, though undoubtedly variable (see their light curves in Figure 10), are most probably not of SX Phe type. However, since their periods exceed 0.1 days, we cannot truly determine their nature. We thus confirm SX-Phe-type fundamental mode pulsations for 10 new variables (namely, SX2, SX3, SX4, SX8, SX10, SX11, SX14, SX21, SX22, SX25) and probable higher pulsation mode for 5 new variables: SX6, SX9_1, SX16, SX17, and SX24. The phase and time-domain light curves of all 21 stars are shown in Figure 10 and their parameters are given in Table 6. The positions of 15 confirmed SX Phe stars on the CCD image are given in Figure 1.

Given the results of our study, the number of confirmed SX Phe stars in M53 reaches 27: 12 previously reported (with the exclusion of V81, V82, and V83) plus 15 discovered by us, and it is quite possible that there are much more still undiscovered. SX Phe stars in GCs can have very short periods (down to 0.025 days) and very small amplitudes; for example, 25% of 149 SX Phe stars in the Rodríguez & López-González (2000) catalog have amplitudes of $< 0\overset{m}{.}05$. Thus, we cannot exclude the possibility that many of the apparently non-varying stars in the SX Phe region vary but with amplitudes too low for us to detect. More sensitive observations are required to search for this exciting class of variables.

4.6.2. RR Lyrae Candidates

We tentatively classify the variable candidates with a characteristic light curve shape as RR Lyrae variables (Clement et al. 2001). The light curves of these 14 RR Lyrae candidates are shown in Figure 11. The equatorial coordinates (α, δ) of these stars, mean brightness in R, and a possible variability type are given in Table 7.

4.6.3. Eclipsing Binaries Candidates

Though about 14% of the nearly 200 BSSs in this cluster are estimated to be in binary systems (Beccari et al. 2008), no eclipsing binary was ever found. Here we report the discovery of 10 short-period contact eclipsing binaries. Kaluzny (1997) noted that almost all known eclipsing main-sequence binaries with periods shorter than about 0.4 days show EW-type light curves.[6] All our suspected W-UMa-type candidates have half-periods of 0.13 days on average and indeed mostly display EW-type light curves. Their equatorial coordinates and light curve parameters are presented in Table 8. For each star we provide designation, equatorial coordinates (α, δ), mean brightness in R, rough estimate of the period, range of variability Δr, epoch of light-minimum T = JD − 2,455,280, and in the Notes we present a possible variability type or BSS match. The phase and time-domain curves are presented in Figure 12.

4.6.4. Unclassified Candidates

In addition to the unclassified variable candidates discussed previously in Sections 3.1.1, 3.2, and 4.6.1, we have found 27 more stars that show definite light variations, but which are also impossible to classify due to the short span of our observations and their possible long periods and irregular nature. Their variability, however, is undoubtful judging from their light curves (Figure 13). The equatorial coordinates and standard R magnitudes of these variables are presented in Table 9. Several of these stars were matched to the BSS catalog by Beccari et al. (2008, Table 10). Stars VC16 and VC24 are possible LPVs, following the method described in Hartman et al. (2004) in which a star is defined as an LPV when a light curve is better fitted by a parabola than by a straight line. In Table 9 is also given the data on V80_7 (see Section 3.2).

4.7. Blue Stragglers in M53

We have cross-correlated the coordinates of the known and newly discovered variables with the BSS database of M53 by Beccari et al. (2008; also G. Beccari 2011, private communication) and found 23 matches within 0.1 arcsec. Seven cases are matches with previously known variables, of which

[6] According to the new GCVS catalog classification, EW stands for a W-Ursa-Majoris (W UMa)-type eclipsing binary.

Table 9
Equatorial Coordinates (α, δ) and Light Curve Parameters for New Unclassified Variable Stars in M53

Variable Designation	α(2000) (h:m:s)	δ(2000) (° :′:″)	$\langle R\rangle$ (mag)	Remarks
VC1	13:12:43.85	18:10:13.0	17.090	LPV
VC2	13:12:50.58	18:10:18.9	18.499	LPV
VC3	13:12:50.66	18:09:39.3	18.298	BSS acs#201010
VC5	13:12:52.26	18:10:21.3	18.975	
VC6	13:12:52.45	18:09:37.3	18.862	
VC7	13:12:52.50	18:10:13.6	19.127	RRl?
VC8	13:12:52.83	18:10:00.8	18.828	
VC9	13:12:53.36	18:09:31.6	18.432	
VC10	13:12:53.61	18:09:54.4	17.603	
VC11	13:12:54.44	18:10:31.2	18.693	
VC12	13:12:54.76	18:10:10.4	17.858	
VC13	13:12:55.32	18:10:21.7	17.240	BSS pc#100221
VC14	13:12:55.42	18:10:39.0	19.128	
VC15	13:12:55.71	18:09:57.0	18.465	BSS pc#103181
VC16	13:12:55.84	18:10:35.5	17.278	LPV
VC17	13:12:56.05	18:09:59.5	18.465	BSS pc#103149
VC18	13:12:56.38	18:10:52.1	20.064	
VC19	13:12:56.43	18:10:57.7	20.145	
VC20	13:12:56.59	18:10:47.5	16.591	
VC21	13:12:55.07	18:09:27.9	19.203	CV?
VC22	13:12:59.98	18:09:24.8	19.439	BSS acs#101000, CV?
VC24	13:12:57.66	18:10:50.0	19.842	LPV
VC25	13:12:58.02	18:09:06.8	19.779	
VC26	13:12:58.03	18:09:03.1	18.130	EB?
VC27	13:12:58.07	18:09:23.5	18.703	
VC28	13:12:53.09	18:10:08.7	19.077	SX Phe? BSS acs#1200729
V80_7	13:12:55.53	18:09:56.9	19.575	See Section 3.2

Table 10
Blue Stragglers in M53

Cat#BSS	Variable Name	$\langle R\rangle$ (mag)	$P_{\rm LK}$ (d)	Type	Remarks
lbc#208210	V74	19.054	0.045055	SX Phe	First report by DK
lbc#219783	V75	19.455	0.044178	SX Phe	New match
lbc#213681	V76	19.434	0.041467	SX Phe	First report by DK
lbc#231344	V79	19.183	0.046255	SX Phe	First report by DK
lbc#208804	V89	19.435	0.043278	SX Phe	New match
acs#100489	V87	19.356	0.046855	SX Phe	New match
pc#102387	V57	16.702		?	See Section 3.1.1
acs#200309	SX4	19.450	0.049500	SX Phe	New
acs#200279	SX6	18.117	0.044755	SX Phe	New
acs#200174	SX9_1	18.573	0.054056	SX Phe	New
acs#1200685	SX14	18.684	0.071130	SX Phe	New
acs#100512	SX17	18.008	0.040567	SX Phe	New
acs#100732	SX19	19.304	0.044378	SX Phe	New
acs#100681	SX21	19.568	0.037762	SX Phe	New
lbc#238275	SX2	19.602	0.039362	SX Phe	New
lbc#240911	SX3	18.786	0.059824	SX Phe	New
acs#100496	W9	19.369	0.152667	W UMa?	New
acs#101000	VC22	19.439	0.24482	CV?	New
acs#201010	VC3	19.713	0.121557	?	New
acs#1200729	VC28	19.080	0.065629	?	New
pc#100221	VC13	17.237	0.177668	?	New
pc#103181	VC15	18.470	0.188068	?	New
pc#103149	VC17	18.463	0.185700	SX Phe?	New

Notes. Column 1 is the star number from the BSS catalog (Beccari et al. 2008). For previously known SX Phe we retained the usual nomenclature (Clement et al. 2001). New BSSs are designated as follows: SX means SX-Phe-type stars, W means W-UMa-type stars, and VC stands for variable candidate (type yet unidentified). $P_{\rm LK}$ means the period was obtained using the LK method (see Section 4.4) and in some cases is only approximate due to the short span of our observations.

four, V57, V75, V87, and V89, are reported by us for the first time (Table 1), and 16 are matches with newly discovered ones. Out of them, nine are SX Phe stars, one is a W UMa candidate, one is a possible LPV, and five are of uncertain type. All stars matched by us with BSSs are shown in Table 10. For each star we provide the BSS catalog number from the Beccari et al. (2008) nomenclature, our designation, mean brightness in R, period determined in this work, and possible variability type, and in the Remarks we indicate who reported the match first. A study in which these new BS stars are analyzed by combining both Beccari et al.'s (2008) and our catalogs is in progress.

5. CONCLUSION

We carried an all-night observation of the GC NGC 5024 (M53) using the 2 m HCT telescope of the IIA in Hanle, India. As a result, we obtained 101 R-band images of the cluster. The reduction of our data using the pre-released version of the DanDIA pipeline (Bramich 2008) revealed significant short-term brightness variations in ∼300 stars. Sixty-six of them are candidates for new variables, out of which fifteen are SX Phe stars (our conclusion was based on the periods, shapes of light curves, and analysis of the $P-L$ relation), ten are W-UMa-type eclipsing binaries (the conclusion is based on the shapes of the light curves) and fourteen are RR Lyrae candidates (the conclusion is based on the shapes of the light curves). The remaining 27 are of yet uncertain type due to our short observational run; because of the limited span of observations, the reliable determination of periods was limited to periods of $\leqslant$0.1 days. Our results constitute the largest population of variables discovered in one research work on M53. Compared to the latest photometric study of this cluster by Dekany & Kovacs (2009), our photometry depth reaches 21 mag in R, and has better precision and better resolution. Consequently, we were able to identify many more new variables and, in a few cases, clarify the status of previously reported ones. We have shown that some previously known variables are misidentified, and some are even non-variable. We refined the equatorial coordinates for all previously known variables in our FOV and provided the equatorial coordinates and finding charts for newly discovered variable candidates. We also report the error in the listing of the M53 variable coordinates in the online catalog of Samus.

Our study shows that M53 may well be the fifth richest GC in variables and, most importantly, second only to ω Cen in the number of SX Phe stars; however, we feel that we have barely scratched the surface. Extensive tests would be necessary to answer the question about the number of variables missed. We are confident that with the advent of new differential imaging techniques, using the 2 m class telescopes and regular observations with moderate cadence, it will be possible to discover many more variables in this cluster.

We are very grateful to Daniel Bramich for providing the DanDIA pipeline to us and giving permission to use it in this work. We also thank D. Bramich and A. Ferro for their help in running it. We thank G. Beccari for kindly sending us the BSS catalogs. We also thank the anonymous referee for insightful and helpful remarks and comments that helped improve this paper.

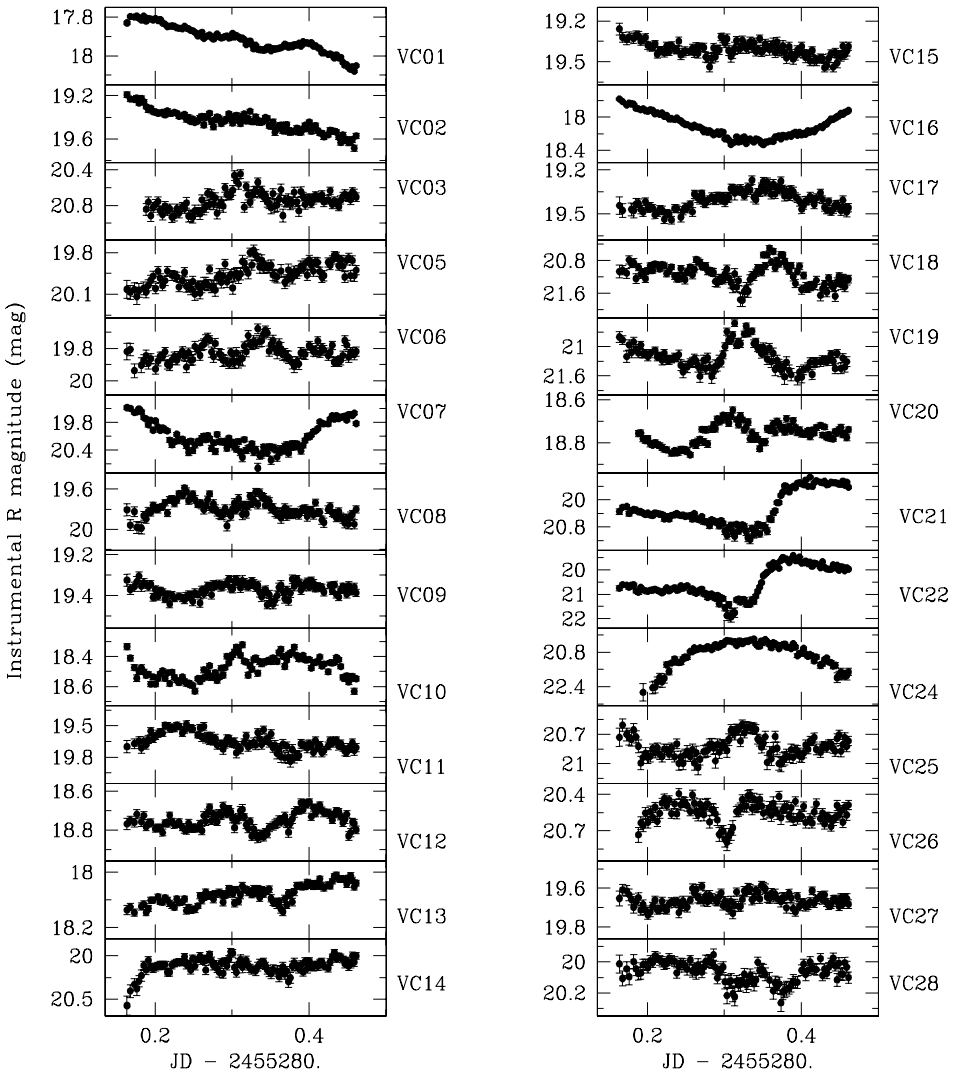

Figure 13. Light curves of unclassified variables labeled with their designations as given in Table 9.

Authors acknowledge the support provided by the staff at the Indian Astronomical Observatory, Hanle and CREST, Hoskote.

REFERENCES

Alard, C. 2000, A&AS, 144, 363
Alard, C., & Lupton, R. H. 1998, ApJ, 503, 325
Arellano Ferro, A., Giridhar, S., Rojas López, V., et al. 2008, RevMexAA, 44, 365
Beccari, G., Lanzoni, B., Ferraro, F. R., et al. 2008, ApJ, 679, 712
Bramich, D. M. 2008, MNRAS, 386, L77
Bramich, D. M., Figuera Jaimes, R., Giridhar, S., & Arellano Ferro, A. 2011, MNRAS, 413, 1275
Bramich, D. M., Horne, K., Bond, I. A., et al. 2005, MNRAS, 359, 1096
Clement, C. M., Muzzin, A., Dufton, Q., et al. 2001, AJ, 122, 2587
Cook, K. H., Alcock, C., Allsman, R. A., et al. 1997, in Variable Stars and the Astrophysical Returns of Microlensing Surveys, ed. R. Ferlet, J.-P. Maillard, & B. Raban (Gif-sur-Yvetle Cedex: Editions Frontieres), 17
Dekany, I., & Kovacs, G. 2009, A&A, 507, 803
Dinescu, D. I., van Altena, W. F., Girard, T. M., & López, C. E. 1999, AJ, 117, 277
Evstigneeva, N. M., Samus', N. N., & Alcaino, G. 1997, Astron. Lett., 23, 395
Harris, W. E. 1996, AJ, 112, 1487
Hartman, J. D., Bakos, G., Stanek, K. Z., & Noyes, R. W. 2004, AJ, 128, 1761
Hartman, J. D., Gaudi, B. S., Holman, M. J., et al. 2008, ApJ, 675, 1254
Jeon, Y., Lee, M. G., Kim, S., & Lee, H. 2003, AJ, 125, 3165
Jeon, Y.-B., Lee, M. G., Kim, S.-L., & Lee, H. 2004, AJ, 128, 287
Kaluzny, J. 1997, A&AS, 122, 1
Kopacki, G. 2000, A&A, 358, 547
Lafler, J., & Kinman, T. D. 1965, ApJS, 11, 216
Lomb, N. R. 1976, Ap&SS, 39, 447
McNamara, D. H. 2000, PASP, 112, 1096
Monet, D. G., Levine, S. E., Canzian, B., et al. 2003, AJ, 125, 984
Nandra, K., George, I. M., Mushotzky, R. F., Turner, T. J., & Yaqoob, T. 1997, ApJ, 476, 70
Pepper, J., Stanek, K. Z., Pogge, R. W., et al. 2008, AJ, 135, 907
Press, W. H., Teukolsky, S. A., Vetterling, W. T., & Flannery, B. P. 1992, Numerical Recipes in FORTRAN, The Art of Scientific Computing (2nd ed.; Cambridge: Cambridge Univ. Press)
Rey, S.-C., Lee, Y.-W., Byun, Y.-I., & Chun, M.-S. 1998, AJ, 116, 1775
Rodríguez, E., & López-González, M. J. 2000, A&A, 359, 597
Safonova, M., & Shastri, P. 2010, Ap&SS, 325, 47
Safonova, M., & Stalin, C. S. 2010, New Astron., 15, 450
Samus, N. N., Kazarovets, E. V., Pastukhova, E. N., Tsvetkova, T. M., & Durlevich, O. V. 2009, PASP, 121, 1378
Schlegel, D. J., Finkbeiner, D. P., & Davis, M. 1998, ApJ, 500, 525
Stetson, P. B. 2000, PASP, 112, 925
Tamuz, O., Mazeh, T., & North, P. 2006, MNRAS, 367, 1521
Vaughan, S., Edelson, R., Warwick, R. S., & Uttley, P. 2003, MNRAS, 345, 1271
Zinn, R. 1985, ApJ, 293, 424